



OPEN ACCESS

EDITED BY

Wenling Tian,
China University of Mining and
Technology, China

REVIEWED BY

Pengju An,
Ningbo University, China
Jinrong Cao,
China University of Mining and
Technology, China

*CORRESPONDENCE

Tengfei Deng,
✉ tengfei.deng@doktorand.tu-freiberg.de

RECEIVED 15 January 2025

ACCEPTED 20 March 2025

PUBLISHED 02 April 2025

CITATION

Deng T (2025) Poroelastic effects on seismic
monitoring in partially saturated loosely
deposited sands.

Front. Earth Sci. 13:1561168.

doi: 10.3389/feart.2025.1561168

COPYRIGHT

© 2025 Deng. This is an open-access article
distributed under the terms of the [Creative
Commons Attribution License \(CC BY\)](#). The
use, distribution or reproduction in other
forums is permitted, provided the original
author(s) and the copyright owner(s) are
credited and that the original publication in
this journal is cited, in accordance with
accepted academic practice. No use,
distribution or reproduction is permitted
which does not comply with these terms.

Poroelastic effects on seismic monitoring in partially saturated loosely deposited sands

Tengfei Deng*

Institute of Geotechnics, Technische Universität Bergakademie Freiberg, Freiberg, Germany

Introduction: A better understanding of the relationship between water saturation and seismic characteristics of loosely deposited sand is crucial for assessing the liquefaction potential of open-pit mine dumps. The classic elastic models, based on Gassmann's theory, are commonly used to constrain water saturation from seismic data. However, while effective at low frequencies, these models fail to capture macroscopic wave-induced fluid flow and poroelastic effects at higher frequencies, which may hinder the application of laboratory results to field conditions. In contrast, Biot's poroelastic theory enables seismic wave propagation modeling across a broad frequency range.

Methods: To evaluate poroelastic effects in seismic monitoring, we compare elastic and poroelastic models in terms of wave velocities, Poisson's ratio, P-wave travel time, and surface wave dispersion across different frequencies. Our study incorporates numerical simulations and experimental data to assess the extent of discrepancies between these models.

Results: Our findings show that the poroelastic model predicts seismic wave velocities with up to a 6% difference compared to the elastic model. While minimal differences are observed in field-scale surveys, the discrepancies become more significant in pilot plant experiments and ultrasonic measurements as frequency increases. These results highlight the influence of poroelastic effects, which are not captured adequately by elastic models at higher frequencies.

Discussion: The observed frequency-dependent discrepancies suggest that elastic models may be insufficient for high-frequency seismic applications. This underscores the need for improved methodologies that integrate poroelastic effects to enhance the scalability of laboratory findings to field conditions.

KEYWORDS

forward seismic modeling, seismic monitoring, loosely deposited sands, poroelastic effects, frequency-dependent

1 Introduction

Open-pit lignite mining operations often create mine dumps composed of loosely deposited sands with high porosity and permeability. The risk of liquefaction in these dumps increases when water levels rise due to rainfall or other factors, posing significant environmental and geotechnical challenges. The degree of saturation in these sands is crucial in assessing the liquefaction potential (Molina-Gómez et al., 2023). Therefore, accurate estimation of the spatial distribution of saturation in loosely deposited sands is essential to map the risk of liquefaction.

Seismic methods provide a non-invasive technique that can cover large areas quickly and efficiently to explore the saturation distribution in loosely deposited sediments. These methods can complement other techniques such as time-domain reflectometry (Fenta and Szanyi, 2021), remote sensing (Mohanty, 2013; Plati et al., 2020), and ground-penetrating radar (Moghadas et al., 2010) to obtain a comprehensive understanding of subsurface conditions (Milani et al., 2015; Solazzi et al., 2021). Successful monitoring of saturation distribution requires proper modeling of the physical properties of porous media, which provides a quantitative link between the physical properties of the media and the seismic response. Loosely deposited sand, being a highly porous medium, necessitates that the physical model accounts for poroelastic effects due to the interaction between soil particles and pore fluid, which impacts wave propagation. A common approach is to use the Gassmann theory (Gassmann, 1951; Wood, 1955) in the elastic model to emphasize fluid effects (Morency et al., 2011), which, based on the low-frequency assumption, is widely used in practical applications such as shallow sediment exploration (Bachrach and Nur, 1998; Bachrach et al., 1998; 2000; Accaino et al., 2023), reservoir engineering (Chen and Zhang, 2017; Wang et al., 2022), and geofluid discrimination (Zong et al., 2015), as it simplifies the modeling of seismic wave propagation in porous media.

However, the elastic model is invalid in the high-frequency range as it cannot model the macroscopic wave-induced fluid flow, i.e., poroelastic effects in the high-frequency range. Meanwhile, seismic methods often rely on empirical correlations established in the laboratory for seismic inversion at the field scale. Correlating lab seismic data with field data provides a necessary database for constructing seismic models of specific geological areas. The frequency used in the lab is usually in the ultrasonic range (high-frequency range), where the mode of poroelastic effects differs from the seismic frequency range (low-frequency range). In this context, the poroelastic model (Biot, 1956a; Biot, 1956b) may be more appropriate for predicting the behavior of porous media across a wide frequency range, which also can incorporate more detailed information during parameterization and inversion compared to the elastic model. This has led to its use in various applications, including seismic exploration (Morency et al., 2011; Anthony and Vedanti, 2020; Alajmi et al., 2023), earthquake engineering (Meng et al., 2022), and soil dynamics (Chen et al., 2020). Furthermore, the poroelastic model has been extended and modified to account for complex phenomena such as anisotropy (Huang et al., 2022; Guo et al., 2022), heterogeneity (Wenzlau, 2009), and nonlinear behavior (Yang et al., 2021). Despite its advantages, the application of the poroelastic model in monitoring shallow sedimentary layers remains limited as the complexity of the environmental conditions, e.g., stiffness and saturation strongly depend on the depth in typical soils (Crane, 2013).

In this regard, some scholars have established the relationship between the seismic characteristics and the relevant properties of shallow loose media in the lab based on the poroelastic model, e.g., Emerson and Foray (2006); Whalley et al. (2012); Linneman et al. (2021). However, the measurement of seismic wave characteristics in lab sample tests provides only a single data point, which cannot be directly compared to field survey results, e.g., P-wave travel time curves, and consider both the pressure dependence of the initial elastic modulus and

the saturation distribution under practical conditions. Lab small-scale physical models using non-contact ultrasound techniques offer new perspectives for monitoring the saturation distribution in the shallow loose media (Bodet et al., 2010; 2014; Pasquet et al., 2016). Although some small-scale physical experiments have demonstrated the applicability of the poroelastic model in the ultrasonic frequency range (e.g., Barrière et al., 2012), there is still lacking. However, a comprehensive theoretical model for partially saturated seismic wave propagation in partially saturated, loosely deposited sands to establish a connection between is still lacking, hindering the extrapolation of small-scale experimental results to field-scale observations. This limitation arises due to the frequency-dependent nature of poroelastic effects, as different frequency ranges are employed in small-scale physical experiments and field-scale observations. Therefore, it is necessary to compare the results between the elastic model and applications. To address this, we used the elastic model as a baseline and compared its predictions with those of the poroelastic model to investigate highlight the impact of poroelastic effects on seismic monitoring data in across different frequency ranges. Additionally, the theoretical model must account for the depth dependence of both the initial elastic modulus and the saturation distribution.

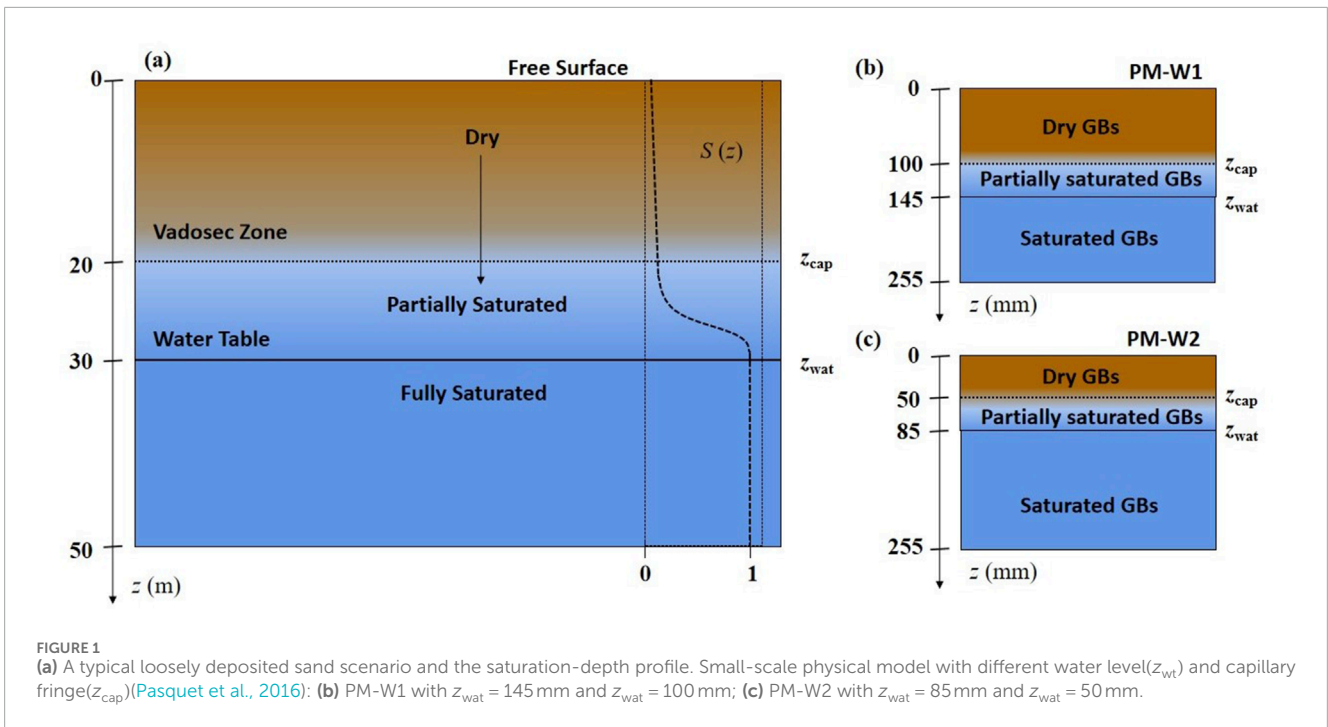
This paper aims to numerically explore poroelastic effects on seismic monitoring data in loosely deposited sands. To this end, we combine the poroelastic model saturated with two immiscible fluids and the Hertz-Mindlin model, considering the saturation-depth profile, to get profiles of V_p and V_s which allow for the simulation of seismic monitoring datasets with different groundwater level, i.e., Poisson's ratio, P-wave travel time and surface-wave dispersion. To evaluate the impact of poroelastic effects on seismic monitoring, we conducted three different scales of monitoring at varying water levels: field survey (seismic frequency), pilot plant survey (sonic frequency), and ultrasonic measurements (ultrasonic frequency). The elastic model serves as the baseline for comparison with the poroelastic model, highlighting poroelastic signatures across different frequency ranges.

2 Methodology

2.1 Background

In a typical open-pit mine dump scenario consisting of loosely deposited sands, as Figure 1a, the vadose zone exhibits varying degrees of saturation ranging from dry to partially saturated, while below the groundwater level, the sediment is fully saturated (Bachrach and Mukerji, 2012). Moreover, due to the complex seismic response of partially saturated loosely deposited sands, a small-scale physical model can be employed to validate relevant theories and media models. For instance, Pasquet et al. (2016) used a lab-scale controlled physical model (PM) consisting of glass beads (GBs), employing the ultrasonic technology to test the sensitivity of seismic monitoring results to different water table levels (Figures 1b, c).

As the model exhibits anisotropy only in the vertical direction, we consider a one-dimensional column of loosely deposited sand with properties dependent on the depth z , such as saturation, density, stiffness, and permeability. This model can be discretized into a stack of n homogeneous and isotropic layers with thickness



h_j , where $j = 1, \dots, n$. The V_{pj} and V_{sj} values for each layer can be obtained through plane wave solution (Morency and Tromp, 2008) of elastic and poroelastic models.

2.2 Calculation of V_p and V_s

In this section, we present the poroelastic model considering the depth dependence of stiffness and saturation. For completeness and reference, a detailed summary of the derivation process of plane wave solution is presented in supplemental materials.

2.2.1 Governing equations of poroelastic model

Wave propagation in porous media (Biot, 1956a; Biot, 1956b) is formulated in terms of the primary variables solid skeleton displacement \mathbf{u} , relative fluid displacement \mathbf{w} and pore pressure p . The equilibrium equation of the porous media is formulated, as presented in Equations 1–4.

$$\rho \ddot{\mathbf{u}} + \rho_f \ddot{\mathbf{w}} = (H - G + \alpha^2 M) \nabla (\nabla \cdot \mathbf{u}) + G \nabla^2 \mathbf{u} + \alpha M \nabla (\nabla \cdot \mathbf{w}) \quad (1)$$

where ρ_f , ρ_s and ρ are the densities of fluid, solid skeleton, and porous media, respectively, with $\rho = \phi \rho_f + (1 - \phi) \rho_s$; ϕ is the porosity of the porous media; $\ddot{\mathbf{u}}$ and $\ddot{\mathbf{w}}$ are the acceleration of the solid skeleton and fluid (relative to solid), respectively; H and μ are the P-wave modulus and shear modulus, respectively, with $H = K + 3/4G$; K and G are bulk modulus and shear modulus of the porous media, respectively; α is Biot's coefficient, with $\alpha = 1 - K/K_s$ (Biot and Willis, 1957; Zienkiewicz, 1982); K_s is the bulk modulus of solid grain; M is the inverse of the storage coefficient, with $M = (\phi/K_f + (\alpha - \phi)/K_s)^{-1}$ (Chang and Yoon, 2018).

The equilibrium equation of fluid is written as

$$\rho_f \ddot{\mathbf{u}} + m \ddot{\mathbf{w}} + b F(t) * \dot{\mathbf{w}} = \alpha M \nabla (\nabla \cdot \mathbf{u}) + M \nabla (\nabla \cdot \mathbf{w}) \quad (2)$$

where $m = \tau \rho_f / \phi$ is the coupling mass and τ is the tortuosity with $\tau = 1 + 0.5(1/\phi - 1)$; $b = \mu_f / k_f$ is the viscous damping parameter; μ_f is the viscosity of the fluid and k_f is the permeability of the fluid.

In Biot's theory, the poroelastic effects is frequency-dependent, which could be characterized by the viscodynamic factor in the frequency domain (Barrière et al., 2012):

$$\tilde{F}(\omega) = \sqrt{1 + \frac{2i\omega}{\omega_c}} \quad (3)$$

where ω_c is the critical frequency in Biot's theory, given by:

$$\omega_c = \frac{\phi \mu_f}{k_f \tau \rho_f} \quad (4)$$

In low-frequency conditions, i.e., $\omega/\omega_c \ll 1$, the pressure gradients generated within the fluid are transmitted to the solid via viscous drag, resulting in no relative motion between the fluid and the solid skeleton, called purely elastic wave regime. This behavior is consistent with Gassmann's theory (Gassmann, 1951), an elastic theory of fluid substitution.

2.2.2 Stiffness modulus of loosely deposited sands

In order to model the wave propagation characteristic in granular material, the Hertz-Mindlin model (Mavko et al., 2009) is employed to assess the stiffness modulus of the soil frame. The bulk and shear modulus are defined in Equations 5, 6, displayed as

$$K = \left[\frac{N^2 (1 - \phi)^2 G_s^2}{18 \pi^2 (1 - \nu_s)^2 P_e} \right]^{1/3} \quad (5)$$

and

$$G = \frac{5 - 4\nu_s}{5(2 - \nu_s)} \left[\frac{3N^2 (1 - \phi)^2 G_s^2}{2\pi^2 (1 - \nu_s)^2 P_e} \right]^{1/3} \quad (6)$$

where the ν_s is the solid grain Poisson's ratio; the average number of contacts per grain $N = 9$; G_s is the shear modulus of the solid grain. The stiffness of loose deposited media is strongly dependent on the effective overburden stress P_e , which is governed not only in terms of overburden stress, saturation, and pore pressure but also especially in terms of capillary pressure, which has been observed in many field measurement and laboratory experiments. Thereby, an expression of effective stress considering capillary pressure is proposed in Equation 7 (Solazzi et al., 2021):

$$P_e = \sigma_z - (1 - S_{ew})p_g - S_{ew}(p_g - p_c) \quad (7)$$

where $\sigma_z = \rho g z$ is the overburden stress; $p_g = \rho_g g z$ is the gas pore fluid pressure; p_c is the capillary pressure; The effective saturation of water is defined as $S_{ew} = (S_w - S_{w,r}) / (1 - S_{w,r})$; S_w is the water saturation and $S_{w,r}$ is the water residual saturation.

2.2.3 Effective fluid properties

The properties of the fluid mixture with water and gas can be evaluated in Equations 8–13. According to the work of Berryman (Berryman et al., 1988), the effective compressibility of fluid can be represented by the average of water and air compressibility (Wood, 1955):

$$\frac{1}{K_f} = \frac{1 - S_w}{K_g} + \frac{S_w}{K_w} \quad (8)$$

where K_g is the gas bulk modulus and K_w is the water bulk modulus. Considering the interaction between the pore gas and water, the relative permeability functions depend on saturation (Barrière et al., 2012), specifically

$$k_{rw} = S_{ew}^{1/2} [1 - (1 - (S_{ew})^{1/m_c})^{m_c}]^2 \quad (9)$$

and

$$k_{rg} = (1 - S_{ew})^{1/2} [1 - (S_{ew}^{1/m_c})]^{2m_c} \quad (10)$$

were chosen here. m_c is the fitting parameters. Effective permeability is defined as consisting of gas and water relative permeability:

$$k_f = k_{f0} (k_{rw} + k_{rg}) \quad (11)$$

where k_{f0} is the intrinsic permeability. An effective viscosity can be obtained from water and gas viscosity following (Berryman et al., 1988):

$$\mu_f = \frac{\mu_w \mu_g}{\mu_w k_{rg} + \mu_g k_{rw}} \quad (12)$$

where μ_g is the viscosity of the gas and μ_w is the viscosity of the water. Meanwhile, for the mixture of two-phase fluid, the fluid density is a linear average of each component, given by

$$\rho_f = \rho_g (1 - S_w) + \rho_w S_w \quad (13)$$

where ρ_g and ρ_w are densities of gas and water, respectively.

2.2.4 Saturation profile

The saturation profile is employed in this paper to consider the variation of saturation with depth. If the capillary pressure at the groundwater table is set as 0, and the depth at Earth's surface is set as 0, according to the well-known van Genuchten's model (Van Genuchten, 1980), the saturation-depth relationship is expressed in Equation 14:

$$S_{ew} = \begin{cases} \{1 + [\alpha_{vg}(z_w - z)]^{n_c}\}^{-m_c} & \text{for } z < z_w \\ 1 & \text{for } z \geq z_w \end{cases} \quad (14)$$

where m_c and n_c are the exponent parameters related to the pore size distribution, with $m_c = 1 - 1/n_c$; α_{vg} is the pressure scaling parameter. Afterward, the capillary pressure expression with depth

$$p_c = \rho_w g (z_w - z) \quad (15)$$

could be obtained. From Equation 15, the capillary pressure profile is only related to the groundwater table. Nevertheless, since the contribution of capillary pressure to the effective pressure is also dependent on the saturation profile, this model can still be applied for extensive to more silty and clayey soils.

2.3 Seismic monitoring indicators

There are three indicators employed to assess the poroelastic effects on seismic monitoring in loosely deposited sands, i.e., Poisson's ratio (Equation 16), P-wave travel time curve (Equations 17–19) and surface wave dispersion curves.

2.3.1 Poisson's ratio

In the field of near-surface geophysics, borehole probing is a commonly employed technique for detecting groundwater tables. However, its large-scale applicability may be constrained by financial and other factors. Seismic surveys are used to acquire the spatial distribution of V_p and V_s in subsurface structures (Grelle and Guadagno, 2009). The equivalent Poisson's ratio is then utilized to differentiate between partially saturated and fully saturated soils, aiding in the determination of the groundwater table location (Uyanik, 2011; Pasquet et al., 2015; Flinchum et al., 2020). This method effectively complements borehole measurements. According to the model setup process, the equivalent Poisson's ratio for each layer can be defined as (Mavko et al., 2009):

$$\nu = \frac{V_{pj}^2 - 2V_{sj}^2}{2(V_{pj}^2 - V_{sj}^2)} \quad (16)$$

where the values of V_{pj} and V_{sj} can be calculated through the plane wave analysis presented in Appendix A. In near-surface applications, the P-wave velocity profile can be inverted using the seismic refraction method, while the S-wave velocity profile can be estimated through surface wave dispersion analysis.

2.3.2 P-wave travel time curve

In general, the seismic refraction method can be applied to detect the saturation distribution of loosely deposited sands due to the sensitivity of P-wave velocity to saturation (Berryman et al., 2002). In shallow seismic refraction surveys, the P-wave travel time

curve includes the direct wave in the near field and the refracted wave in the far field. Consider a layer of thickness h and velocity V_1 overlying a uniform halfspace with velocity V_2 , where $V_1 < V_2$. The arrival times at point x for the direct and refracted waves, t_{dir} and t_{refr} , are given by:

$$t_{\text{dir}} = \frac{x}{V_1} \quad (17)$$

and

$$t_{\text{refr}} = \frac{x}{V_2} + \frac{2h\sqrt{V_2^2 - V_1^2}}{V_1 V_2}. \quad (18)$$

In this paper, the 1D model is discretized into a sufficient number of layers with equal thickness Δh . For multiple layers, the seismic energy at each interface is refracted according to Snell's law. The intercept of the refraction travel time is controlled by the root mean square (RMS) velocity of all the layers above the reflector, defined as

$$V_{\text{rms}} = \sqrt{\frac{\sum_{i=1}^n V_i^2 \Delta t_i}{\sum_{i=1}^n \Delta t_i}} \quad (19)$$

where Δt_i is the two-layer travel time for seismic energy propagating perpendicular through the i -th layer. The V_1 in Equation 18 can be replaced by the RMS velocity.

2.3.3 Surface wave dispersion analysis

Surface wave dispersion analysis is a non-invasive geophysical technique used to quantitatively assess frequency-dependent changes in the phase velocities of surface waves (Foti et al., 2011; Mi et al., 2018; Zhang et al., 2020). This method primarily relies on the properties of Rayleigh waves (Elias and Alderton, 2020), which result from the superposition of wave propagation between different subsurface media interfaces. As the wavelength shortens and the depth of penetration increases, wave velocity varies with frequency, exhibiting a dispersive phenomenon. This dispersion is related to the physical properties of the subsurface, such as density, compressibility, and shear resistance. Consequently, analyzing the surface wave dispersion curve provides valuable insights into the characteristics and structure of the subsurface.

Rayleigh waves are primarily driven by S-waves (Flinchum et al., 2020), which typically increase with depth in loosely deposited sands. In surface wave dispersion analysis, the phase velocity at lower frequencies reflects the deeper S-wave velocity structure, while higher frequencies reveal the shallow structure (Flinchum et al., 2020). Consequently, the surface wave dispersion curve can be utilized to invert and obtain the 1D S-wave profile (Pasquet and Bodet, 2017). In this study, we investigate the influence of different models on the surface-wave dispersion curve across various scales. To construct surface-wave dispersion curves, the `dispa` python library¹ is employed for the forward modeling of surface-wave dispersion.

1 <https://github.com/keurfonluu/dispa>

3 Results and discussion

In this section, we numerically investigate the poroelastic effects on seismic monitoring in loosely deposited sands across various scale applications (corresponding to different frequency ranges). We first study the poroelastic effects on the velocities of P- and S-waves with different saturation degrees in the ultrasonic frequency range, where the macroscopic wave-induced fluid flow happens. Then we explore the poroelastic effects on the Poisson's ratio, P-wave travel time, and surface wave dispersion with different frequency ranges.

3.1 Poroelastic effects on V_p and V_s

In the following, we first validate the model employing two sets of lab sample experimental results and briefly illustrate the influence of poroelastic effects on body wave propagation characteristics with different saturation degrees.

3.1.1 Experiment 1

The first experimental study (Barrière et al., 2012) examines the effects of saturation (ranging from 0.1 to 0.9) on the characteristics of the fast P wave in an unconsolidated porous medium. Wave velocity and attenuation are determined using plane wave analysis, with material parameters listed in Table 1 (Exp.1). Additionally, the energy losses due to friction between sand particles are considered in the energy dissipation analysis. In natural soils and rocks, internal damping, known as hysteretic damping, is independent of frequency. The Constant-Q model is commonly used to characterize this

TABLE 1 Physical properties of soils employed in the numerical experiments.

Variable	Unit	Exp.1	Exp.2
ρ_s	kg m ⁻³	2,650	2,650
ρ_w	kg m ⁻³	1,000	1,000
ρ_g	kg m ⁻³	1.2	1.2
K_s	Pa	3.6×10^{10}	3.6×10^{10}
K_w	Pa	2.2×10^9	2.2×10^9
K_g	Pa	1.0×10^5	1.0×10^5
K	Pa	2.5×10^7	1.0×10^8
G	Pa	1.2×10^7	4.6×10^7
ϕ	--	0.4	0.43
k_{f0}	m ²	1×10^{-12}	3×10^{-7}
μ_w	Pa • s	1×10^{-3}	1×10^{-3}
μ_g	Pa • s	1×10^{-5}	1×10^{-5}
S_{wr}	--	0.085	0.085

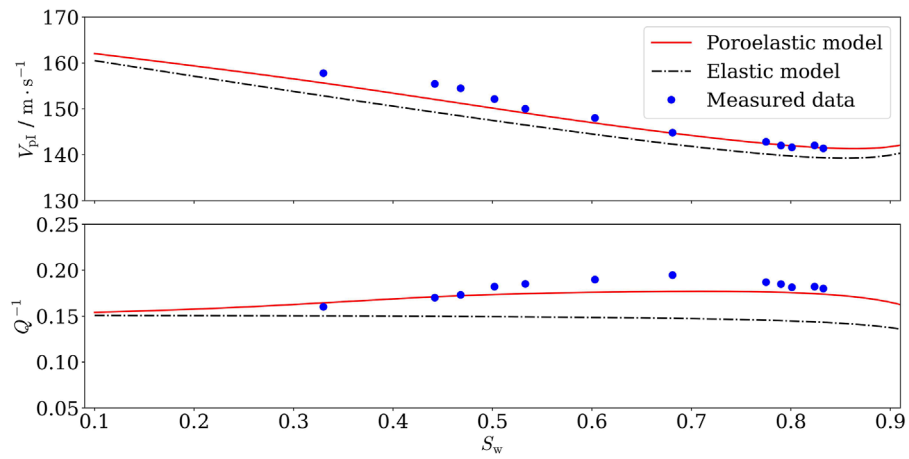


FIGURE 2 Effect of saturation on fast P wave propagation characteristics (exciting frequency 1.8kHz): velocity of fast P-wave (upper) and inverse quality factor (bottom).

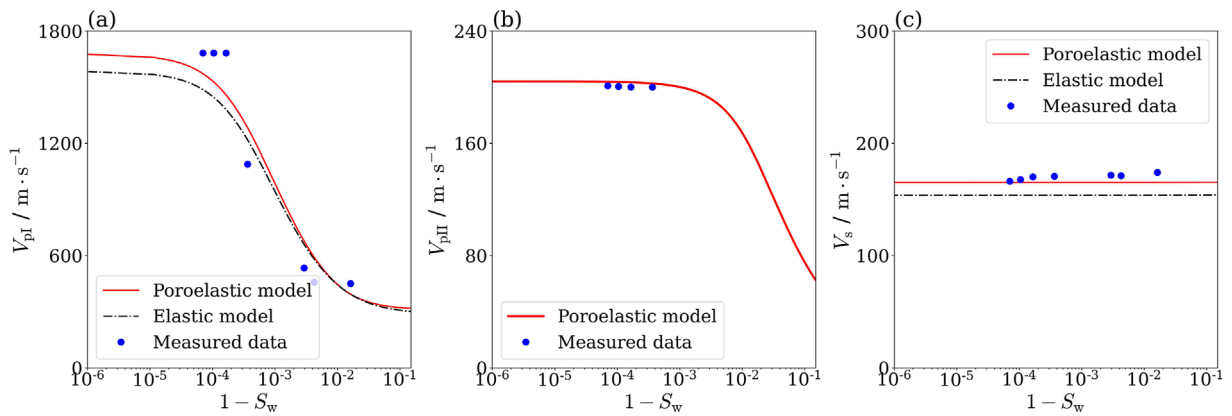


FIGURE 3 Effect of saturation on body wave velocities (exciting frequency 10kHz): (a) fast P-wave; (b) slow P-wave; (c) S-wave.

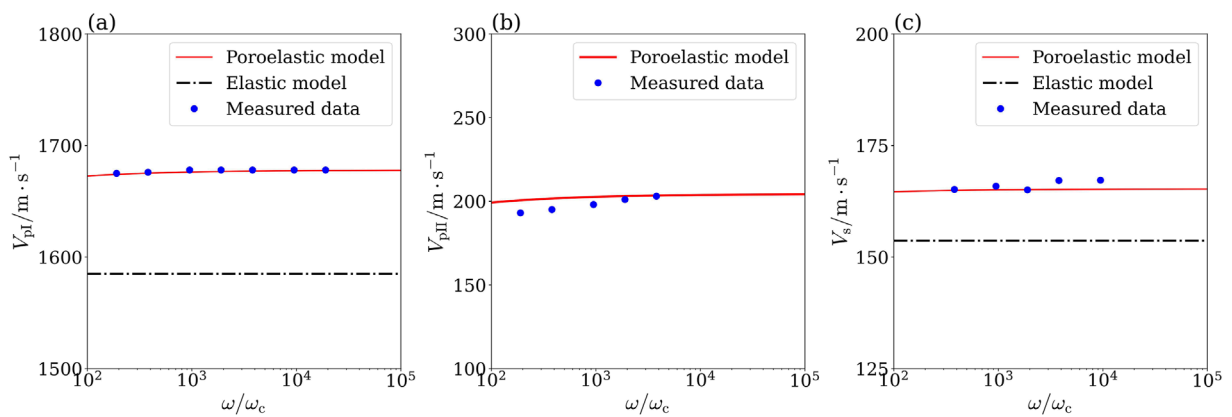
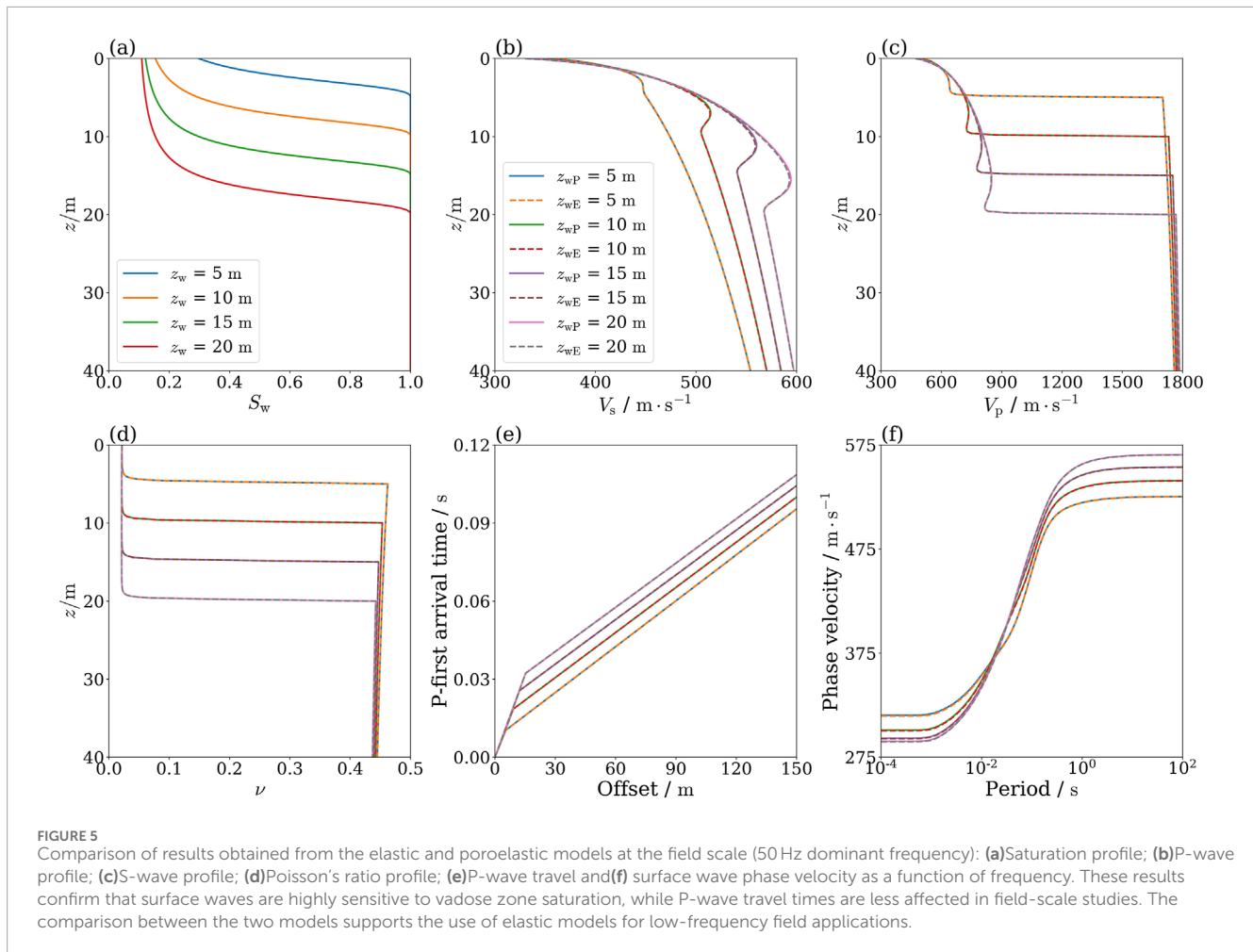


FIGURE 4 Effect of frequency on body wave velocities in full saturation state: (a) fast P-wave; (b) slow P-wave; (c) S-wave.



behavior across all frequency ranges (Carcione, 2015). The frequency-dependent stiffness modulus is expressed in Equations 20, 21 (Barrière et al., 2012):

$$K^* = K * \left(i \frac{\omega}{\omega_0} \right)^{2\gamma_K} \quad (20)$$

$$G^* = G * \left(i \frac{\omega}{\omega_0} \right)^{2\gamma_G} \quad (21)$$

where $\omega_0/2\pi = 2.0$ kHz is the reference frequency of the Constant-Q model. The exponent parameters related to the quality factor for stiffness modulus losses, $\gamma_K = 0.038$ and $\gamma_G = 0.062$ in this simulation.

Figure 2 illustrates the effect of saturation on the fast P-wave velocity and wave attenuation. From those figures, it can be seen that the poroelastic model agrees better with the experimental data compared to the elastic model, which demonstrates the favorable predictive capability of the poroelastic model for fast P-wave characteristics. This discrepancy is attributed to the inability of Gassmann's theory to accurately characterize the poroelastic effects at the exciting frequency (1.8 kHz). Besides, the wave velocity exhibits a slight decrease as saturation increases, possibly due to the increased effective density of porous media.

3.1.2 Experiment 2

In the first experiment, the model was studied within a saturation range, from 0.1 to 0.9. However, the properties of fluid undergo significant changes when saturation is close to 1.0 (Whalley et al., 2012). Therefore, it is necessary to investigate the wave propagation characteristics in the near-saturated range (approximately 0.9–1.0). Gu et al. (2021) conducted a series of laboratory specimen tests using the bender element, where Fujian sand was oven-dried before sample preparation, and all specimens underwent compaction to ensure material homogeneity. Moreover, carbon dioxide flushing ensuring complete displacement of air and back pressure changing were employed to achieve high saturation and vary the saturation levels, respectively. All parameters used in the simulation are listed in Table 1 (Exp.2).

Figure 3 show the effect of saturation on fast P-wave, slow P-wave, and S-wave. The simulation results obtained from the poroelastic model generally align with the measured data except for some discrepancies attributed to the selected parameters (Gu et al., 2021), with some discrepancies. These deviations are primarily due to parameter selection. For instance, the shear modulus used in the theoretical prediction was derived from S-wave measurements taken when the soil was nearly saturated (Gu et al., 2021). Additionally, the definition of effective permeability and viscosity influences the critical frequency, contributing to the observed differences.

TABLE 2 Physical properties of soils for application studies.

Variable	Unit	Value
ρ_s	kg m ⁻³	2,650
ρ_w	kg m ⁻³	1,000
ρ_g	kg m ⁻³	1.2
K_s	Pa	4.5×10^{10}
G_s	Pa	3.6×10^{10}
K_w	Pa	2.2×10^9
K_g	Pa	1.0×10^5
ϕ	--	0.42
k_{f0}	m ²	5.0×10^{-11}
η_w	Pa • s	1×10^{-3}
η_g	Pa • s	1×10^{-5}
$S_{w,r}$	–	0.085
n_c	–	2.78

Moreover, the elastic model fails to predict the existence of the slow P-wave as it can not model macroscopic wave-induced fluid flow. As saturation is close to 1.0, the velocity of the fast P-wave changes significantly due to sharp variations in the fluid properties. From Figure 3a, it can be observed that the predictive ability of the elastic model is comparable to the poroelastic model with saturation near 99.9%. This may be due to the dominance of changes in fluid properties as opposed to poroelastic effects.

For a better understanding of the poroelastic effect on seismic wave velocities in the high-frequency regime where pressure gradients in the fluid only serve to accelerate fluid motion, we compared the model predictions with experimental data in the fully saturated state, as shown in Figure 4. From those figures, it can be found there is a better agreement between the model predictions and the measured data. As shown in Figures 4a, c, there is a significant discrepancy of up to 6% between the elastic model and the poroelastic model, indicating the inability of the elastic model to characterize the poroelastic effect in the high-frequency regime.

3.2 Poroelastic effects on seismic monitoring in field surveys

According to Section 2, the dominant frequency of the source, set at 50 Hz, establishes a purely elastic wave regime wherein there is no relative motion between the fluid and solid matrix. The static water table depth is assumed as 5 m, 10 m, 15 m and 20 m, yielding four distinct saturation profiles which can be determined by Equation 15 with a specific value $\alpha_{vg} = 0.442 \text{ m}^{-1}$, as shown in Figure 5a. The other parameters are listed in Table 2.

Figures 5b–d display the profiles of P-wave, S-wave, and Poisson's ratio in the low-frequency range, respectively. From those figures, it can be found that there is a general consistency in the predictions of both poroelastic and elastic models, which has been validated through various field measurements, e.g., Bachrach and Nur (1998); Flinchum et al. (2020). It can be noted that both P- and S-wave velocity profiles exhibit a minor inflection point characterized by a localized decrease in velocity near the water table. This phenomenon can be attributed to a sudden increase in the effective density of the medium prior to the full saturation. As shown in Figure 5b, the P-wave velocity undergoes a sudden increase close to the water level. This is due to the abrupt alteration of the effective fluid bulk modulus K_f . Besides, Poisson's ratio also has a sharp increase near the water table, while maintaining relative constancy in both unsaturated and saturated zones. This makes it possible to determine the location of the water table in the shallow subsurface using Poisson's ratio profile although it falls short in adequately characterizing saturation changes from a continuous water table to the ground surface (Solazzi et al., 2021).

Figure 5e demonstrate the curves of P-wave travel time with different water tables. It is noticed from this figure the predicted results of the poroelastic model agree with the elastic model. This suggests that both models possess comparable predictive capabilities in the low-frequency range. Comparing the travel time curve among various water tables, it can be seen that there is a similarity in slopes among direct wave travel time curves which suggests that P-wave velocity remains relatively unaffected by saturation levels in the unsaturated region. The difference among the travel-time curves stems from fluctuations in the location of the water table. The slope of refracted wave travel time curves remains consistent, indicating that P-wave velocities near water table depths are basically the same. This is because P-wave velocity is mainly governed by the fluid in shallow loose media consistent with Figure 5c.

Figure 5f shows the surface wave velocity dispersion as a function of frequency simulated by the elastic and poroelastic models. From this figure it is noted that there is a notable agreement concerning surface wave velocity dispersion between two models. It also can be found that surface wave dispersion is significantly influenced by the alterations in the water table. By comparing the outcomes of different water tables, it is found there is notable variability in the low-frequency (high period) range indicating variations in the deep medium structure, e.g., water table location. Furthermore, in the high-frequency range (low period), it is observed discernible differences among the results of different saturation profiles. This suggests surface waves are responsive to changes in saturation of the vadose zone, while this sensitivity is not shown in the P-wave travel time curves.

3.3 Poroelastic effects on seismic monitoring in pilot plant surveys

For intermediate frequencies with regard to the ratio ω/ω_c , as it is the case for a source dominant frequency of 1.0 kHz in the model with the pilot plant surveys, the inertia force and the viscous shearing act simultaneously. The four different saturation profiles are shown in Figure 6a with $\alpha_{vg} = 8.84$. The other parameters are listed in Table 2.

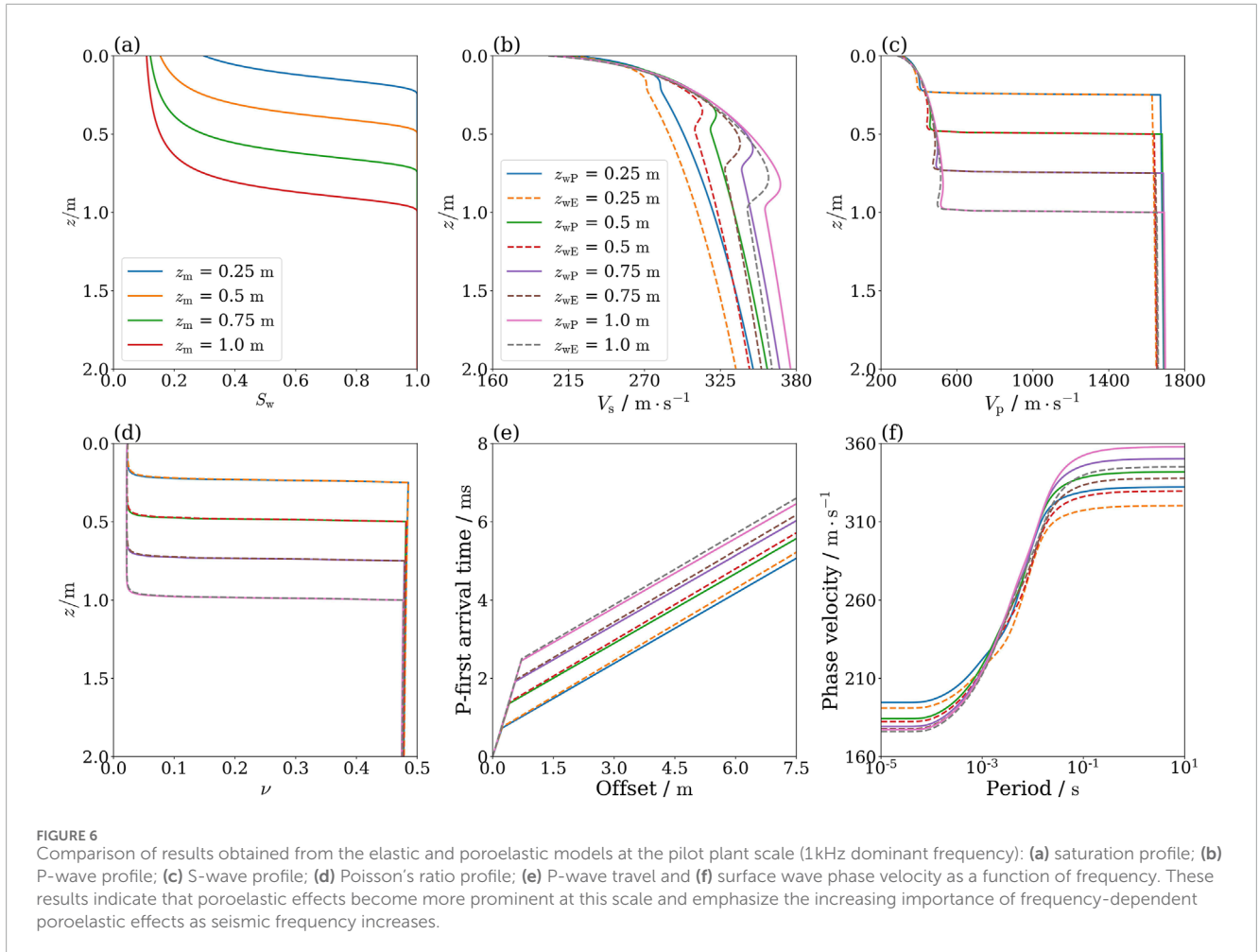


Figure 6b, c display the P- and S-wave velocity profiles of elastic and poroelastic models in the intermediate-frequency range. It can be seen from those figures that the poroelastic and elastic modeling results are broadly similar in the low saturation region, while a clear divergence occurs in the high saturation region. This divergence stems from the lower velocity dispersion observed at low saturation and higher at high saturation. Figure 6d shows the Poisson's ratio profiles with different water table levels. There exists only a minor discrepancy between the outcomes of elastic and poroelastic models. This suggests that the influence of poroelastic effects on Poisson's ratio profiles remains relatively consistent across low and intermediate-frequency conditions.

Figure 5e describes the P-wave travel time curves for the elastic and poroelastic models with different water table levels. From this figure, it can be seen that the major difference between the two models is in the refraction band, even though it is not significant. An indication of the apparent velocity near the water table is given by the slope of the refraction curve. Therefore, the velocity dispersion in the intermediate-frequency range are not sufficient to cause significant changes in the apparent velocity. Moreover, in the direct band region, both models produce nearly identical predictions due to minimal velocity dispersion in the unsaturated range.

Figure 5f illustrates the surface wave dispersion curves for the elastic and poroelastic models with different water table levels. It

can be seen from this figure that there is a significant difference between the predictions of the two models, especially in the low-frequency region (high period). This observation indicates that the elastic model fails to adequately capture the poroelastic effects in the intermediate frequency range. Furthermore, in the high-frequency region (low period), there is also a marked difference between the predictions of the two models. Even though it is not as pronounced as in the low-frequency region, this finding further highlights the limitations of the elastic models.

3.4 Poroelastic effects on seismic monitoring in ultrasonic measurements

For high frequencies with regard to the ratio ω/ω_c , as is the case for a source dominant frequency of 10kHz in the model with the ultrasonic measurements, the pressure gradients on the fluid only contribute to accelerating the fluid motion. The four different saturation profiles are shown in Figure 7a with $\alpha_{vg} = 88.4$. The other parameters are listed in Table 2.

Figure 7b, c show the P- and S-wave velocity profiles for the elastic and poroelastic models in the high-frequency range. It is clear from these figures that there is a significant difference between the elastic and poroelastic models in the prediction

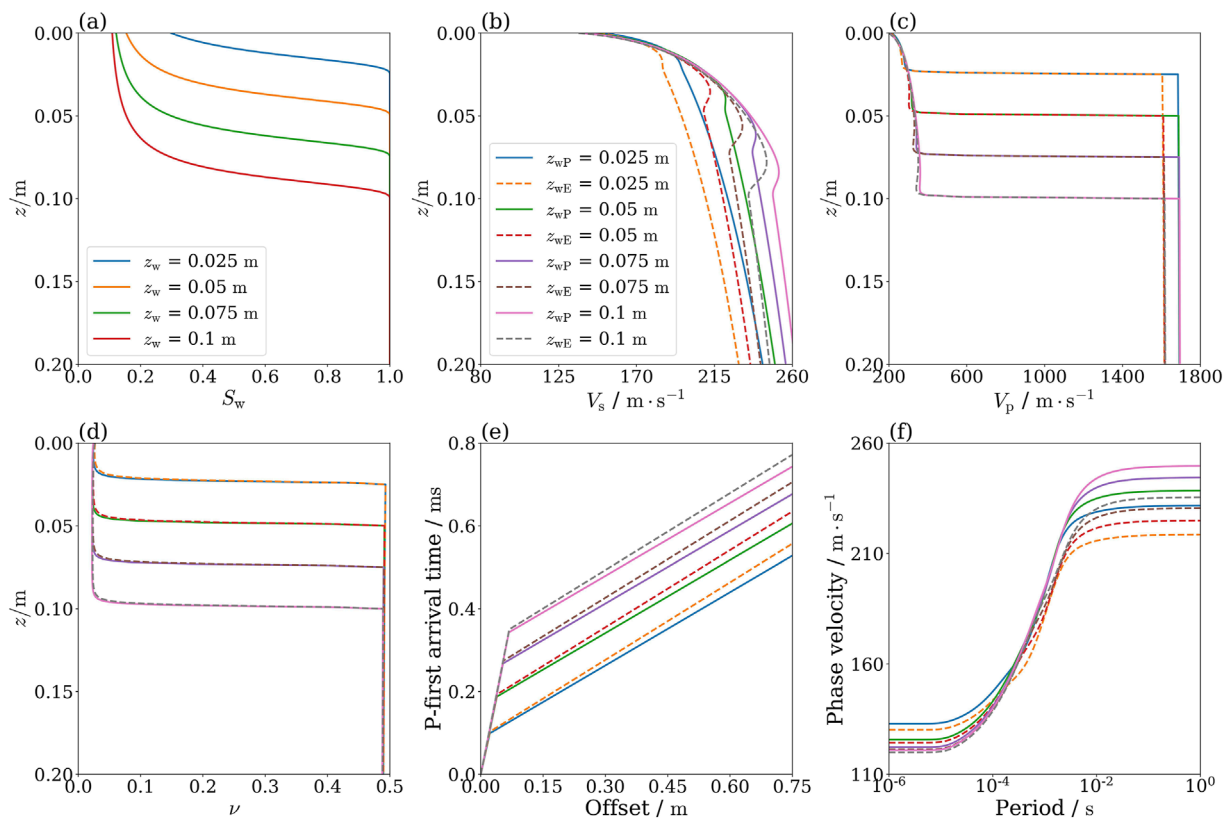


FIGURE 7 Comparison of results obtained from the elastic and poroelastic models at the ultrasonic scale (10kHz dominant frequency): (a) Saturation profile; (b) P wave profile; (c) S wave profile; (d) Poisson's ratio profile; (e) P-wave travel and (f) surface wave phase velocity as a function of frequency. These findings reinforce the conclusion that ultrasonic-scale experiments are not directly transferable to field applications and suggest that laboratory-scale measurements may need additional corrections when applied to real scenarios.

of body wave velocity profiles. Compared to the intermediate-frequency range, this difference becomes more apparent as the frequency increases. These observations suggest that the poroelastic effects on body waves is frequency-dependent. Figure 7d presents the Poisson's ratio profiles of the elastic and poroelastic models for different water table conditions. It is worth noting that the results remain consistent regardless of which model or frequency range is chosen, as described in the previous section. A plausible explanation for the wave velocity dispersion is the frequency-dependent nature of the inertial interaction mass (Carcione, 2015). It is apparent that the Poisson's ratio or V_p/V_s is independent of the mass.

Figure 7e demonstrates the P-wave travel time curves for elastic and poroelastic models with different water table levels. It can be seen there is a significant decrease in the slope of the refractive section. This is due to the larger velocity dispersion in the high-frequency range. Figure 7f shows the surface wave dispersion curves for the elastic and poroelastic models with different water table levels. Compared to the pilot-scale results, the variability in the predictions of both models increases significantly, indicating that the lab results are not directly transferable to field application.

4 Conclusion

In this study, we investigate the impact of poroelastic effects on seismic monitoring results. The poroelastic signature is derived by contrasting elastic and poroelastic models. Based on the obtained results, the following conclusions can be drawn:

- (1) A comparison of two sets of laboratory data investigates the poroelastic effects on body wave velocities. Besides, the inability of the elastic model to capture porous elastic effects in the high-frequency range is briefly illustrated. In low saturation conditions, the poroelastic effect exhibits a small frequency dependence, whereas the opposite is true in high saturation conditions, especially in the case of full saturation.
- (2) Different frequencies typically correspond to applications at different scales (seismic site surveys, pilot plant surveys, and ultrasonic measurements). The Poisson's ratio profile is an effective way to detect water table levels at various scales. Besides, the frequency-dependent poroelastic effect

mainly affects the refractive wave band and surface wave dispersion curve.

- (3) Seismic monitoring results exhibit high sensitivity to changes in water level, suggesting the feasibility of utilizing time-lapse seismic methods to monitor saturation distribution in loosely deposited sands.

These findings highlight the discrepancies in seismic monitoring results across different frequency ranges and can serve as a basis for parameterization across applications at various scales. However, some limitations of this work should be acknowledged. While the poroelastic effects on seismic monitoring results have been confirmed by comparing elastic and poroelastic models, more experimental data with different scales are needed for further validation. Additionally, incorporating the poroelastic effects involve only macroscopic wave-induced fluid flow in this paper. Incorporating the heterogeneous fluid distribution in porous media may provide insight into the poroelastic effects on seismic wave propagation distribution-induced mesoscopic wave-induced fluid flow in poroelastic effects may provide more realistic predictions, especially for applications in natural sediments and mine tailings. Moreover, future research could explore the use of machine learning techniques to improve poroelastic parameter estimations. Recent studies have demonstrated that deep learning approaches can effectively infer complex subsurface properties from seismic data. Applying such methods to poroelastic modeling could enhance parameter inversion accuracy and reduce computational costs. In addition, the model could be extended to assess geohazards, e.g., liquefaction (Molina-Gómez et al., 2023) and landslides (Li et al., 2024; Fang et al., 2023).

Data availability statement

The raw data supporting the conclusions of this article will be made available by the authors, without undue reservation.

Author contributions

TD: Conceptualization, Data curation, Funding acquisition, Investigation, Software, Validation, Visualization, Writing – original draft, Writing – review and editing.

References

- Accaino, F., Col, F., Böhm, G., Picotti, S., Giorgi, M., Meneghini, F., et al. (2023). Petro-physical characterization of the shallow sediments in a coastal area in ne Italy from the integration of active seismic and resistivity data. *Surv. Geophys.* 44, 1211–1238. doi:10.1007/s10712-023-09776-x
- Alajmi, M., Gei, D., Carcione, J., Qadrouh, A., and Ba, J. (2023). Methodology to monitor the seismic response to injected carbon dioxide: model and synthetic seismograms of CO₂ injection. *Acta Geophys.* 72, 1343–1353. doi:10.1007/s11600-023-01199-x
- Anthony, E., and Vedanti, N. (2020). Simulation of seismic wave propagation in poroelastic media using vectorized biot's equations: an application to a CO₂ sequestration monitoring case. *Acta Geophys.* 68, 435–444. doi:10.1007/s11600-020-00414-3
- Bachrach, R., Dvorkin, J., and Nur, A. (1998). High-resolution shallow-seismic experiments in sand, part ii: velocities in shallow unconsolidated sand. *Geophysics* 63, 1234–1240. doi:10.1190/1.1444424
- Bachrach, R., Dvorkin, J., and Nur, A. (2000). Seismic velocities and Poisson's ratio of shallow unconsolidated sands. *Geophysics* 65, 559–564. doi:10.1190/1.1444751
- Bachrach, R., and Mukerji, T. (2012). *Analysis of 3D high-resolution seismic reflection and crosswell radar tomography for aquifer characterization: a case study*. Houston, Texas: SEG library, 607–620.
- Bachrach, R., and Nur, A. (1998). High-resolution shallow-seismic experiments in sand, part i: water table, fluid flow, and saturation. *Geophysics* 63, 1225–1233. doi:10.1190/1.1444423
- Barrière, J., Bordes, C., Brito, D., Sénéchal, P., and Perroud, H. (2012). Laboratory monitoring of p waves in partially saturated sand. *Geophys. J. Int.* 191, 1152–1170. doi:10.1111/j.1365-246X.2012.05691.x
- Berryman, J., Berge, P., and Bonner, B. (2002). Estimating rock porosity and fluid saturation using only seismic velocities. *Geophysics* 67, 391–404. doi:10.1190/1.1468599

Funding

The author(s) declare that financial support was received for the research and/or publication of this article. The authors thank the support from the China Scholarship Council (CSC) project (No. 201906430070).

Acknowledgments

We thank all reviewers for valuable comments, and the Frontiers Editorial Office for improving the layout of this Research Topic.

Conflict of interest

The author declares that the research was conducted in the absence of any commercial or financial relationships that could be construed as a potential conflict of interest.

Generative AI statement

The author(s) declare that no Generative AI was used in the creation of this manuscript.

Publisher's note

All claims expressed in this article are solely those of the authors and do not necessarily represent those of their affiliated organizations, or those of the publisher, the editors and the reviewers. Any product that may be evaluated in this article, or claim that may be made by its manufacturer, is not guaranteed or endorsed by the publisher.

Supplementary material

The Supplementary Material for this article can be found online at: <https://www.frontiersin.org/articles/10.3389/feart.2025.1561168/full#supplementary-material>

- Berryman, J. G., Thigpen, L., and Chin, R. C. Y. (1988). Bulk elastic wave propagation in partially saturated porous solids. *J. Acoust. Soc. Am.* 84, 360–373. doi:10.1121/1.396938
- Biot, M. A. (1956a). Theory of propagation of elastic waves in a fluid-saturated porous solid. i. low-frequency range. *J. Acoust. Soc. Am.* 28, 168–178. doi:10.1121/1.1908239
- Biot, M. A. (1956b). Theory of propagation of elastic waves in a fluid-saturated porous solid. ii. higher frequency range. *J. Acoust. Soc. Am.* 28, 179–191. doi:10.1121/1.1908241
- Biot, M. A., and Willis, D. G. (1957). The elastic coefficients of the theory of consolidation. *J. Appl. Mech.* 24, 594–601. doi:10.1115/1.4011606
- Bodet, L., Dhemaied, A., Martin, R., Mourgues, R., Rejiba, F., and Tournat, V. (2014). Small-scale physical modeling of seismic-wave propagation using unconsolidated granular media. *Geophysics* 79, T323–T339. doi:10.1190/geo2014-0129.1
- Bodet, L., Jacob, X., Tournat, V., Mourgues, R., and Gusev, V. (2010). Elasticity profile of an unconsolidated granular medium inferred from guided waves: toward acoustic monitoring of analogue models. *Tectonophysics* 496, 99–104. doi:10.1016/j.tecto.2010.10.004
- Carcione, J. M. (2015). *Wave fields in real media*. third edition edn (Oxford: Elsevier).
- Chang, K. W., and Yoon, H. (2018). 3-D modeling of induced seismicity along multiple faults: magnitude, rate, and location in a poroelasticity system. *J. Geophys. Res. Solid Earth* 123, 9866–9883. doi:10.1029/2018JB016446
- Chen, H., and Zhang, G. (2017). Estimation of dry fracture weakness, porosity, and fluid modulus using observable seismic reflection data in a gas-bearing reservoir. *Surv. Geophys.* 38, 651–678. doi:10.1007/s10712-017-9410-x
- Chen, W., Jeng, D., Chen, W., Chen, G., and Zhao, H. (2020). Seismic-induced dynamic responses in a poro-elastic seabed: solutions of different formulations. *Soil Dyn. Earthq. Eng.* 131, 106021. doi:10.1016/j.soildyn.2019.106021
- Crane, J. M. (2013). *Effects of stress and water saturation on seismic velocity and attenuation in near surface sediments*. Baton Rouge, Louisiana: Louisiana State University and Agricultural and Mechanical College.
- Elias, S., and Alderton, D. (2020). *Encyclopedia of geology*. Elsevier Science.
- Emerson, M., and Foray, P. (2006). Laboratory p-wave measurements in dry and saturated sand. *Acta Geotech.* 1, 167–177. doi:10.1007/s11440-006-0015-7
- Fang, K., Tang, H., Li, C., Su, X., An, P., and Sun, S. (2023). Centrifuge modelling of landslides and landslide hazard mitigation: a review. *Geosci. Front.* 14, 101493. doi:10.1016/j.gsf.2022.101493
- Fenta, M., and Szanyi, J. (2021). Fibre optic methods of prospecting: a comprehensive and modern branch of geophysics. *Surv. Geophys.* 42, 551–584. doi:10.1007/s10712-021-09634-8
- Flinchum, B. A., Banks, E., Hatch, M., Batelaan, O., Peeters, L. J. M., and Pasquet, S. (2020). Identifying recharge under subtle ephemeral features in a flat-lying semi-arid region using a combined geophysical approach. *Hydrology Earth Syst. Sci.* 24, 4353–4368. doi:10.5194/hess-24-4353-2020
- Foti, S., Parolai, S., Albarello, D., and Picozzi, M. (2011). Application of surface-wave methods for seismic site characterization. *Surv. Geophys.* 32, 777–825. doi:10.1007/s10712-011-9134-2
- Gassmann, F. (1951). Elastic waves through a packing of spheres. *GEOPHYSICS* 16, 673–685. doi:10.1190/1.1437718
- Grelle, G., and Guadagno, F. M. (2009). Seismic refraction methodology for groundwater level determination: “water seismic index”. *J. Appl. Geophys.* 68, 301–320. doi:10.1016/j.jappgeo.2009.02.001
- Gu, X., Kangle, Z., Tessari, A., and Gao, G. (2021). Effect of saturation on the characteristics of p-wave and s-wave propagation in nearly saturated soils using bender elements. *Soil Dyn. Earthq. Eng.* 145, 106742. doi:10.1016/j.soildyn.2021.106742
- Guo, J., Zhao, L., Chen, X., Yang, Z., Li, H., and Liu, C. (2022). Theoretical modelling of seismic dispersion, attenuation, and frequency-dependent anisotropy in a fluid saturated porous rock with intersecting fractures. *Geophys. J. Int.* 230, 580–606. doi:10.1093/gji/ggac070
- Huang, X., Greenhalgh, S., Han, L., and Liu, X. (2022). Generalized effective biot theory and seismic wave propagation in anisotropic, poroviscoelastic media. *J. Geophys. Res. Solid Earth* 127, e2021JB023590. doi:10.1029/2021jb023590
- Li, G., Hu, Z., Wang, D., Wang, L., Wang, Y., Zhao, L., et al. (2024). Instability mechanisms of slope in open-pit coal mines: from physical and numerical modeling. *Int. J. Min. Sci. Technol.* 34, 1509–1528. doi:10.1016/j.ijmst.2024.10.003
- Linneman, D. C., Strickland, C. E., and Mangel, A. R. (2021). Compressional wave velocity and effective stress in unsaturated soil: potential application for monitoring moisture conditions in vadose zone sediments. *Vadose Zone J.* 20, e20143. doi:10.1002/vzj2.20143
- Mavko, G., Mukerji, T., and Dvorkin, J. (2009). *The rock physics handbook: tools for seismic analysis of porous media*. 2 edn. Cambridge University Press.
- Meng, K., Cui, C., Xu, C., Wang, B., Xin, Y., and Liang, Z. (2022). Approach for defective floating pile embedded in layered saturated soils and application in pile integrity test. *Int. J. Numer. Anal. Methods Geomechanics* 46, 2893–2912. doi:10.1002/nag.3432
- Mi, B., Xia, J., Shen, C., and Wang, L. (2018). Dispersion energy analysis of Rayleigh and love waves in the presence of low-velocity layers in near-surface seismic surveys. *Surv. Geophys.* 39, 271–288. doi:10.1007/s10712-017-9440-4
- Milani, M., Rubino, J., Ludovic, B., Sidler, R., and Holliger, K. (2015). Attenuation of sonic waves in water-saturated alluvial sediments due to wave-induced fluid flow at microscopic, mesoscopic and macroscopic scales. *Geophys. J. Int.* 146–147. doi:10.1093/gji/ggv287
- Moghadas, D., André, F., Slob, E. C., Vereecken, H., and Lambot, S. (2010). Joint full-waveform analysis of off-ground zero-offset ground penetrating radar and electromagnetic induction synthetic data for estimating soil electrical properties. *Geophys. J. Int.* 182, 1267–1278. doi:10.1111/j.1365-246x.2010.04706.x
- Mohanty, B. P. (2013). Soil hydraulic property estimation using remote sensing: a review. *Vadose Zone J.* 12 (06.0100), 1–9. doi:10.2136/vzj2013.06.0100
- Molina-Gómez, F., Viana da Fonseca, A., Ferreira, C., and Caicedo, B. (2023). Improvement of cyclic liquefaction resistance induced by partial saturation: an interpretation using wave-based approaches. *Soil Dyn. Earthq. Eng.*, 167. doi:10.1016/j.soildyn.2023.107819
- Morency, C., Luo, Y., and Tromp, J. (2011). Acoustic, elastic and poroelastic simulations of CO₂ sequestration crosswell monitoring based on spectral-element and adjoint methods. *Geophys. J. Int.* 185, 955–966. doi:10.1111/j.1365-246x.2011.04985.x
- Morency, C., and Tromp, J. (2008). Spectral-element simulations of wave propagation in porous media. *Geophys. J. Int.* 175, 301–345. doi:10.1111/j.1365-246x.2008.03907.x
- Pasquet, S., and Bodet, L. (2017). Swip: an integrated workflow for surface-wave dispersion inversion and profiling. *Geophysics* 82, WB47–WB61. doi:10.1190/geo2016-0625.1
- Pasquet, S., Bodet, L., Bergamo, P., Guérin, R., Martin, R., Mourgues, R., et al. (2016). Small-scale seismic monitoring of varying water levels in granular media. *Vadose Zone J.* 15, 1–14. doi:10.2136/vzj2015.11.0142
- Pasquet, S., Bodet, L., Dhemaied, A., Mouhri, A., Vitale, Q., Rejiba, F., et al. (2015). Detecting different water table levels in a shallow aquifer with combined p-surface and sh-wave surveys: insights from vp/vs or Poisson's ratios. *J. Appl. Geophys.* 113, 38–50. doi:10.1016/j.jappgeo.2014.12.005
- Plati, C., Loizos, A., and Gkyrtis, K. (2020). Assessment of modern roadways using non-destructive geophysical surveying techniques. *Surv. Geophys.* 41, 395–430. doi:10.1007/s10712-019-09518-y
- Solazzi, S., Bodet, L., Holliger, K., and Jougnot, D. (2021). Surface-wave dispersion in partially saturated soils: the role of capillary forces. *J. Geophys. Res. Solid Earth* 126, e2021JB022074. doi:10.1029/2021jb022074
- Uyanik, O. (2011). The porosity of saturated shallow sediments from seismic compressional and shear wave velocities. *J. Appl. Geophys.* 73, 16–24. doi:10.1016/j.jappgeo.2010.11.001
- Van Genuchten, M. (1980). A closed-form equation for predicting the hydraulic conductivity of unsaturated soils. *Soil Sci. Soc. Am. J.* 44, 892–898. doi:10.2136/sssaj1980.03615995004400050002x
- Wang, P., Cui, Y.-A., and Liu, J. (2022). Fluid discrimination based on inclusion-based method for tight sandstone reservoirs. *Surv. Geophys.* 43, 1469–1496. doi:10.1007/s10712-022-09712-5
- Wenzlau, F. (2009). *Poroelastic Modelling of Wavefields in Heterogeneous Media Poroelastische Modellierung von Wellenfeldern in Heterogenen Medien*. Karlsruhe, Germany: Karlsruhe Institute of Technology.
- Whalley, W., Jenkins, M., and Attenborough, K. (2012). The velocity of shear waves in unsaturated soil. *Soil Tillage Res.* 125, 30–37. doi:10.1016/j.still.2012.05.013
- Wood, A. (1955). *A textbook of sound*. Maryland, United States: Maxwell Press.
- Yang, J., Yang, D., Han, H., Qiu, L., and Cheng, Y. (2021). A wave propagation model with the Biot and the fractional viscoelastic mechanisms. *Sci. China Earth Sci.* 64, 364–376. doi:10.1007/s11430-020-9668-5
- Zhang, X., Roy, C., Curtis, A., Nowacki, A., and Baptie, B. (2020). Imaging the subsurface using induced seismicity and ambient noise: 3-D tomographic Monte Carlo joint inversion of earthquake body wave traveltimes and surface wave dispersion. *Geophys. J. Int.* 222, 1639–1655. doi:10.1093/gji/ggaa230
- Zienkiewicz, O. (1982). Basic formulation of static and dynamic behaviours of soil and other porous media. *Appl. Math. Mech.* 3, 457–468. doi:10.1007/BF01908222
- Zong, Z., Yin, X., and Wu, G. (2015). Geofluid discrimination incorporating poroelasticity and seismic reflection inversion. *Surv. Geophys.* 36, 659–681. doi:10.1007/s10712-015-9330-6